Presence of uranium(V) during uranium(VI) reduction by Desulfosporosinus hippei DSM 8344T

Hilpmann, S.; Roßberg, A.; Steudtner, R.; Drobot, B.; Hübner, R.; Bok, F.; Prieur, D.; Bauters, S.; Kvashnina, K.; Stumpf, T.; Cherkouk, A.;

Originally published:

March 2023

Science of the Total Environment 875(2023), 162593

DOI: https://doi.org/10.1016/j.scitotenv.2023.162593

Presence of uranium(V) during uranium(VI) reduction by *Desulfosporosinus hippei* DSM 8344^T

S. Hilpmann[1], A. Rossberg[1,2], R. Steudtner[1], B. Drobot[1], R. Hübner[3], F. Bok[1], D. Prieur[1,2], S. Bauters[1,2], K. O. Kvashnina[1,2], T. Stumpf[1], A. Cherkouk[1]*

[1]*Helmholtz-Zentrum Dresden-Rossendorf, Institute of Resource Ecology, Bautzner Landstraße 400, 01328 Dresden, Germany*

[2]*Rossendorf Beamline (BM20-ROBL), European Synchrotron Radiation Facility, Grenoble, France*

[3]*Helmholtz-Zentrum Dresden-Rossendorf, Institute of Ion Beam Physics and Materials Research, Dresden, Germany*

*Corresponding author:

Andrea Cherkouk

Email: a.cherkouk@hzdr.de

Phone: +49 351 260 2989

Key words:

Uranium(VI) reduction, sulfate-reducing bacteria, Opalinus Clay pore water, pentavalent uranium, membrane vesicles

Abstract

Microbial U(VI) reduction influences uranium mobility in contaminated subsurface environments and can affect the disposal of high-level radioactive waste by transforming the water-soluble U(VI) to less mobile U(IV). The reduction of U(VI) by the sulfate-reducing bacterium *Desulfosporosinus hippei* DSM 8344^T, a close phylogenetic relative to naturally occurring microorganism present in clay rock and bentonite, was investigated. D. *hippei* DSM 8344^T showed a relatively fast removal of uranium from the supernatants in artificial Opalinus Clay pore water, but no removal in 30 mM bicarbonate solution. Combined speciation calculations and luminescence spectroscopic investigations showed the dependence of U(VI) reduction on the initial U(VI) species. Scanning transmission electron microscopy coupled with energy-dispersive X-ray spectroscopy showed uranium-containing aggregates on the cell surface and some membrane vesicles. By combining different spectroscopic techniques, including UV/Vis spectroscopy, as well as uranium M_4-edge X-ray absorption near-edge structure recorded in high-energy-resolution fluorescence-detection mode and extended X-ray absorption fine structure analysis, the partial reduction of U(VI) could be verified, whereby the formed U(IV) product has an unknown structure. Furthermore, the U M_4 HERFD-XANES showed the presence of U(V) during the process. These findings offer new insights into U(VI) reduction by sulfate-reducing bacteria and contribute to a comprehensive safety concept for a repository for high-level radioactive waste.

1 Introduction

Clay formations are potential host rocks for the long-term storage of high-level radioactive waste in deep geological repositories.[1,2] A multi-barrier system is favored to isolate the waste from the biosphere, consisting of the technical (container with the waste), the geotechnical (sealing and back-filling material, *e.g*. compacted bentonite) and the geological barrier (host rock).[3,4] Different influencing factors have to be taken into account to ensure the long-term safety of such a repository. One of them is the presence of natural microbial communities in these environments which can have an influence on the waste, *e.g.* in a worst-case scenario, if water enters the repository. As a result, microorganisms can interact with the released radionuclides and can influence their mobility by different processes, *e.g.* sorption, accumulation, change in the speciation or reduction/oxidation.[5–7] In the context of these investigations, particular attention will be paid to the change in oxidation states, especially with respect to uranium, which represents the largest fraction of the spent nuclear fuel.

Various studies showed that sulfate-reducing microorganisms, especially *Desulfosporosinus* species, occur in different clay formations, as well as in bentonite.[8,9] An important representative of the genus is *Desulfosporosinus hippei* DSM 8344^T. This bacterium was originally isolated from permafrost soil and identified as *Desulfotomaculum orientis* by Vainshtain *et al*.[10,11] *Desulfotomaculum orientis* was reclassified as *Desulfosporosinus orientis* by Stackebrandt *et al*., 1997.[12] Later on, the genetic and phenotypic attributes of *Desulfosporosinus hippei* DSM 8344^T were investigated and recognized as representing a distinct and novel species within the genus *Desulfosporosinus* (Vatsurina *et al*., 2008).[13] It has been known for some time that various microorganisms can reduce uranium and other metals. In 1991, Lovley *et al*. demonstrated for the first time the reduction of U(VI) to less soluble U(IV) by the Fe(III)-reducing microorganisms *Geobacter metallireducens* and *Shewanella oneidensis*.[14] These bacteria can generate energy for anaerobic growth by reducing U(VI). In addition, various sulfate-reducing microorganisms, for example *Desulfotomaculum reducens*,[15] *Desulfovibrio desulfuricans*[16] and *Desulfovibrio vulgaris*,[17] as well as different other *Desulfovibrio* species,[17–19] are also capable of converting U(VI) to the insoluble U(IV). But not all of them can grow based on energy gain from U(VI) reduction only. U(VI) reduction by the sulfate-reducing bacterium *Desulfotomaculum reducens* MI-1 was investigated via transcriptomics by Junier *et al*.[20] They found the

upregulation of genes encoding for proteins involved in respiration, suggesting that electrons were shuttled to the electron transport chain, which points to the reduction of U(VI) as a metabolic process. Furthermore, genes involved in *c*-type cytochrome biogenesis were upregulated. Additionally, spores of this sulfate-reducer are capable of reducing U(VI) under certain circumstances.[21] Another study showed, that a certain uranium isotopic fractionation is induced by U(VI) reduction by different microbial strains in contrast to chemical uranium reduction.[22] In 2004, Suzuki *et al*. investigated the U(VI) reduction by *Desulfosporosinus* species for the first time.[23,24] The process was studied using *Desulfosporosinus orientis* DSM 765 and *Desulfosporosinus* sp. P3 at a pH of 7 and a U(VI) as well as lactate concentration of 1 mM. A visible reduction of U(VI) by the formation of black-brown precipitates was verified in this study by X-ray absorption near-edge structure (XANES) spectroscopy. It was also shown that these *Desulfosporosinus* species differ significantly from other U(VI)-reducing microorganisms in one particular respect. They were not able to reduce U(VI) in bicarbonate solution. This buffer is preferentially used to study U(VI) reduction by various microorganisms, not only for sulfate-reducers.[14,16–18,25,26] Furthermore, *Desulfosporosinus* spp. do not contain cytochrome c_3,[27] which has been shown to play an important role, but is not the only pathway for U(VI) reduction by sulfate-reducing microorganisms as *e.g*. *Desulfovibrio*.[19,28] Nevertheless, the process of U(VI) reduction by sulfate reducers is not yet completely understood. Therefore, the aim of this study was to get more insights into the occurring interaction mechanisms of the sulfate-reducing microorganism *D. hippei* DSM 8344^T with U(VI) using multiple microscopic and spectroscopic techniques. In order to mimic as closely as possible the natural conditions in a repository for high-level radioactive waste in clay rock, artificial Opalinus Clay pore water solution[29] was employed as a background electrolyte for the reduction experiments, and lower U(VI) concentrations as previously studied were applied. Thus, this work differs significantly from previous reduction studies in which bicarbonate or other buffers were primarily used. As a comparison, some of the studies presented herein were also performed in bicarbonate buffer. The U(IV) formed during reduction is less mobile than the higher oxidation state +VI because U(IV) often forms water-insoluble compounds. Different studies characterized the biogenic products of the U(VI) reduction for various anaerobic microbial genera, *e.g. Shewanella*, *Geobacter*, *Desulfovibrio*, and also *Desulfosporosinus*, and found uraninite as the main product of the process.[24,30–32] In contrast to this, Bernier-Latmani *et al*. showed the formation of different U(IV) products in

dependence on different experimental conditions and used microbial strains (*e.g*. *Shewanella oneidensis*, *Clostridium acetobutylicum*, and *Desulfotomaculum reducens*).[26] In this case, non-uraninite products including different U(IV)-orthophosphates were found in addition to uraninite. Therefore, structural characterization of the reduction products remains a crucial part of an overall reduction study. Furthermore, uranyl(V) seems to play an important role in the reduction process by iron-reducing bacteria, as previously studied for *Shewanella oneidensis* MR1 and *Geobacter sulfurreducens*, as well.[33,34] L_3- and M_4-edge XANES, as well as fluorescence spectroscopy suggest a one-electron transfer as a mechanism for the reduction process.[7,33,34] While other actinyl(V) species, specifically plutonyl(V) and neptunyl(V), are of certain environmental significance,[34–36] the uranyl(V) cation is reported to be relatively unstable due to the occurring disproportionation to U(IV) and uranyl(VI).[37] In contrast to this, recent studies showed the possibility of stabilizing this oxidation state in the presence of different ligands[37–43] or in iron-bearing phases.[44–49] Furthermore, Vettese *et al*. reported a certain stabilization of U(V) during the reduction by *Shewanella oneidensis* MR1.[33] X-ray absorption spectroscopic techniques verified the presence of up to 30% U(V) even after about 120 h.

In this study, we investigated the U(VI) reduction in artificial Opalinus Clay pore water solution by *Desulfosporosinus hippei* DSM 8344^T, an important representative of the microbial communities in clay rock and bentonite. Therefore, a unique combination of different spectroscopic and microscopic techniques was used to get more information about the ongoing processes. The presence of different uranium oxidation states in the samples was verified using UV/Vis spectroscopy, as well as uranium M_4-edge high-energy-resolution fluorescence-detected X-ray absorption near-edge structure (HERFD-XANES spectroscopy.[50,51] Furthermore, new information about the chemical surroundings of the formed uranium reduction products were provided via EXAFS. Time-resolved laser-induced fluorescence spectroscopy (TRLFS) provided more information about the U(VI) speciation in the supernatants. Moreover, different microscopic techniques such as fluorescence microscopy and transmission electron microscopy (TEM) showed the cell viability during the experiment and the uranium localization in the cells. Only by combining these different methods, it is possible to draw a picture of the ongoing processes during the U(VI) reduction. The obtained information will contribute to a comprehensive safety assessment considering microbiological influences for the selection of a final disposal site in clay rock as well as for the use of bentonite as a possible sealing and backfill material.

Additionally, this study provides new findings in the field of bioremediation of contaminated anoxic environments.[52–56]

2 Materials and methods

2.1 Cultivation

D. hippei DSM 8344^T was purchased from the Leibniz Institute DSMZ – German Collection of Microorganisms and Cell Cultures (DSMZ, Braunschweig, Germany). The strain was cultivated in modified DSM 641 medium containing per L: 1 g NH_4Cl, 2 g Na_2SO_4, 1 g $Na_2S_2O_3$ x 5 H_2O, 1 g $MgSO_4$ x 7 H_2O, 0.1 g $CaCl_2$ x 2 H_2O, 0.5 g KH_2PO_4, 2 g $NaHCO_3$, 2.5 g $NaC_3H_5O_3$, 1 g yeast extract, 1 mL trace element solution, 1 mL selenite-tungstate solution, and 25 mg Na_2S. The trace element solution contains per L: 1.5 g $FeCl_2$ x 4 H_2O dissolved in 10 mL HCl (25%), 70 mg $ZnCl_2$, 100 mg $MnCl_2$ x 4 H_2O, 6 mg H_3BO_3, 190 mg $CoCl_2$ x 6 H_2O, 2 mg $CuCl_2$ x 6 H_2O, 24 mg $NiCl_2$ x 6 H_2O, and 36 mg Na_2MoO_4 x 2 H_2O. The selenite-tungstate solution consists of 0.5 g NaOH, 3 mg Na_2SeO_3 x 5 H_2O, and 4 mg Na_2WO_4 x 2 H_2O per liter. Both stock solutions were autoclaved (20 min at 120 °C) for storage.

All components of the medium except the sodium sulfide were dissolved in deionized water. Afterwards, the medium was fumigated for 45 min with a gas mixture of N_2:CO_2 (80:20), because it contains bicarbonate. After autoclaving, the medium was completed by adding a sterile (autoclaved as well) anoxic stock solution of Na_2S. The cultivation was done at 30 °C in the dark. Cells were harvested in the mid exponential growth phase (OD_{600} of about 0.08 – 0.1 after 42 – 48 h of growth, corresponding to cell numbers of $6x10^5$ – $8x10^5$ cells/mL) by anaerobic centrifugation at 10,000 x g and 18 °C for 10 min. For further experiments, cells were washed with anoxic sterile artificial Opalinus Clay pore water solution at pH 5.5 (see 2.2.1) once and resuspended in an appropriate volume of the same solution to obtain a stock suspension with an OD_{600} of 2.5. The optical density of the cell suspension was measured with a Specord® 50 Plus UV/VIS spectrometer from Analytik Jena at a wavelength of 600 nm.

2.2 Uranium(VI) concentrations in the supernatants

2.2.1 Preparation of artificial Opalinus Clay pore water

For the reduction experiments, artificial Opalinus Clay pore water was used as background electrolyte. Its composition was determined by Wersin *et al.*[29] The pore water has the following composition per L: 12.6 g NaCl, 3.8 g $CaCl_2$ x 2 H_2O, 2.0 g Na_2SO_4, 120 mg KCl, 3.5 g $MgCl_2$ x 6 H_2O, 130 mg $SrCl_2$ x 6 H_2O, and 40 mg $NaHCO_3$ (molar concentrations see Table S1). In addition to the natural components 22 mg Na_2S were added to maintain strict anaerobic conditions. For preparation, all components except for the sodium sulfide were dissolved in deionized water and gasified for 45 min with a gas mixture containing N_2:CO_2 (80:20). The pore water was transferred into an anaerobic box with N_2-atmosphere (MB200 B, M. Braun, Munich, Germany), and sodium sulfide was added to the solution as solid compound inside the anaerobic box. The final solution was filled into serum bottles sealed with butyl plugs. The bottles were brought outside the anaerobic chamber, and the atmosphere above the pore water was exchanged for a mixture of 80% nitrogen and 20% carbon dioxide. Afterwards, the artificial Opalinus Clay pore water was autoclaved for 20 min at 121 °C and stored at 4 °C until usage.

2.2.2 Batch experiments

For the U(VI) reduction experiments, the anoxic U(VI) solutions in artificial Opalinus Clay pore water containing either 100 or 500 µM U(VI) and 10 mM sodium lactate at a pH of 5.5 were prepared. If not otherwise stated, the sample volume was 20 mL in 50-mL sealed serum bottles. As electron donor lactate was added for the investigation of a potential reduction of U(VI) to U(IV). Lactate and other organic matter occur in lower concentrations in natural Opalinus Clay pore water.[57] Nevertheless, in these experiments long-term processes present in nature were simulated. Experimentally, however, only much shorter periods can be investigated. Therefore, higher lactate concentrations were used to speed up the processes. Furthermore, such lactate concentrations had been applied before for different kind of U(VI) reduction experiments.[19,33]

U(VI) solutions in 30 mM bicarbonate buffer were prepared in the same way using only 500 µM U(VI) as initial concentration. The pH value of the buffer was around 6.8. The

U(VI) stock solution (0.1 M U(VI) in 0.5 M HCl) used for these experimental solutions was prepared as previously described.[58]

Afterwards, an appropriate amount of the washed cell suspension (in artificial Opalinus Clay pore water or bicarbonate buffer) was added to the solution to achieve an OD_{600} in the samples of 0.1 (dry bio mass (DBM) = 0.044 mg/mL, cell numbers: $8x10^5$ cells/mL). Reference samples with heat-killed cells were prepared via boiling of the cell suspension at 99 °C for 5 min (1 mL aliquots). Viability of the cells was checked by live/dead staining (see 2.4 and Fig S1). Furthermore, an experiment with incubation in the dark was carried out, as well, to exclude the influence of a possible light-mediated U(VI) reduction by lactate. Stability of the U(VI) solution was proven by measuring U concentrations in a cell-free blank solution over time (see Fig S2)

Suspensions were incubated at room temperature in an anaerobic chamber, and samples were taken between 0 h and one week. To determine the U concentration by inductively coupled plasma mass spectrometry (ICP-MS), as well as to determine the sulfate and lactate concentrations, samples were centrifuged for 5 min at 10,000 x g and 18 °C in the anaerobic glove box. Subsequently, 1 mL of the supernatants was acidified with 10 µL of concentrated nitric acid (69%) and the U concentration were determined via ICP-MS as described previously.[59] To determine the sulfate concentration, 1 mL of the supernatants were taken and examined by ion chromatography (integrated ion chromatography system, Thermo Scientific). The lactate concentrations were determined with a sample volume of 250 µl using high pressure liquid chromatography (HPLC system Agilent 1200 with a G1315B 1200 diode array detector). Concentrations were calculated using a calibration curve in the range between 0 and 20 mM. Except when otherwise stated, experiments were performed in triplicate. Not every analytical method was performed in every experiment.

2.3 Time-resolved laser-induced fluorescence spectroscopy

Time-resolved laser-induced fluorescence spectroscopic (TRLFS) measurements of the supernatants were used to investigate the speciation of U(VI) (100 µM) in the supernatants. Samples for TRLFS were taken after 2 h, 4 h, 24 h, and 48 h of incubation time, except when otherwise stated. For sample preparation, 1 mL of each supernatant (after centrifugation at 18 °C and 10,000 x g for 5 min) was transferred into a semi-micro UV/Vis

cuvette in the anaerobic glovebox. Furthermore, a blank solution without cells was prepared, as well.

To enable an assignment of the recorded and evaluated spectra to different chemical species, a lactate reference is necessary. Therefore, a solution of artificial Opalinus Clay pore water containing 100 µM U(VI) and 10 mM sodium lactate at a pH of 5.5 was prepared.

All samples, as well as the blank solution and the reference, were frozen in liquid nitrogen and stored under -80 °C until measurement. Subsequent measurements and data evaluation were carried out according to Bader *et al*.[60] To minimize the quenching effect of the chloride anions (originating from the artificial Opalinus Clay pore water) on the U(VI) luminescence, the measurements were performed at a temperature of 150 K.[61]

2.4 Verification of cell viability

For fluorescence microscopy imaging of uranium-incubated cells, 1 mL of the suspensions were taken and centrifuged anaerobically at 18 °C and 10,000 x g for 5 min. Cells were resuspended in a small amount of anoxic artificial Opalinus Clay pore water. Staining was performed with a LIVE/DEAD® BacLight™ Bacterial Viability Kit (Thermo Fisher Scientific, Waltham, MA, USA) according to the manufacturer's instructions under anaerobic conditions. Cover glasses were sealed with transparent nail polish to avoid oxygen intake during image capture outside the glovebox. Fluorescence was excited by light with wavelengths of 420 and 460 nm. Therefore, filters Cy3 and FITC were applied and images were taken by using a phase-contrast microscope Olympus BX-61 (Olympus Europa Holding GmbH, Hamburg, Germany) with support of the imaging software "CellSense Dimension 1.11.

2.5 Transmission electron microscopy

Transmission electron microscopy (TEM) was used to get more information about the localization of uranium on/in the cells. To enable this, thin sections of the uranium-incubated cells were prepared. Two U(VI) concentrations of 100 and 500 µM and two incubation times (4 h and 24 h) were investigated, as well as a reference without uranium incubation also after 24 h. TEM specimen preparation was performed as previously described

by Völkner *et al*., with the modification that the *en-bloc* staining with uranyl acetate was omitted.[62,63] In particular, the cells were incubated for the respective times as described before (see 2.2.2). Afterwards, samples were centrifuged (18 °C and 10,000 x g for 5 min) and washed in anoxic 0.1 M sodium cacodylate buffer (pH 7.2). The cell pellet was resuspended in 3 mL of an anoxic fixation buffer (0.1 M sodium cacodylate at pH 7.2, containing 2% glutaraldehyde), subsequently. Further processing was done aerobically at the CRTD (Center for Regenerative Therapies Dresden). Semi-thin sections were cut with a Leica UC6 ultra microtome and stained with toluidine blue/borax to identify potential regions of interest, followed by ultrathin sectioning using a diamond knife. The ultrathin sections were collected on carbon-coated slot grids.

Bright-field and high-resolution transmission electron microscopy (TEM) images were recorded with an image-C_s-corrected Titan 80-300 microscope (Field Electron and Ion Company (FEI), Eindhoven, The Netherlands) operated at an accelerating voltage of 300 kV. Furthermore, high-angle annular dark-field scanning transmission electron microscopy (HAADF-STEM) imaging and spectrum imaging analysis based on energy-dispersive X-ray spectroscopy (EDXS) were performed with a Talos F200X microscope equipped with a high-brightness X-FEG electron source and a Super-X EDX detector system at an accelerating voltage of 200 kV (FEI). Prior to each (S)TEM analysis, the ultrathin section mounted in a high-visibility low-background holder was placed for 2 s into a Model 1020 Plasma Cleaner (Fischione, Export, PA, USA) to remove potential contamination.

2.6 UV/Vis spectroscopy

To clearly give proof of the formed U(IV), UV/Vis measurements of the dissolved cell pellets were carried out. Therefore, a total of 60 mL (triplicates of 20 mL sample volume, DBM = 2.64 mg, 4.8×10^7 cells) of the uranium-incubated cell suspension was centrifuged (at 18 °C and 10,000 x g for 10 min) at the respective time points as well as heat-killed cell samples incubated with U(VI) for one week.

Afterwards, the collected cell pellet was dissolved in 4 mL of anoxic 5 M HCl. Meanwhile, the sample was shaken for one hour on a shaking plate at 120 rpm. The suspension was centrifuged at 18 °C and 10,000 x g for 10 min, and the supernatant was transferred into a quartz glass cuvette. To calculate the ratio between U(VI) and U(IV) afterwards, the total

uranium concentrations were determined by ICP-MS measurements for each sample. All work was carried out anaerobically. A Cary 5G UV-Vis-NIR spectro-photometer from Varian was used for the UV/Vis measurement, and the spectrum was recorded in the spectral range between 200 and 800 nm with a minimum step width of 0.1 nm. U(VI) and U(IV) reference spectra were prepared with a concentration of 1 mM uranium in the corresponding oxidation state in 5 M HCl. Both the calculations and the results for all time points are given in the supporting information.

2.7 High-energy-resolution fluorescence-detected X-ray absorption near-edge structure spectroscopy (HERFD-XANES) and extended X-ray absorption fine structure (EXAFS) methods

For extended X-ray absorption fine structure (EXAFS) and high-energy-resolution fluorescence-detected X-ray absorption near-edge structure (HERFD-XANES) spectroscopy, samples were incubated with 100 µM U(VI) for different time points (4 h, 24 h, 48 h, and 168 h). In this case, suspensions with a doubled optical density of 0.2 (1.6×10^6 cells/mL) were used to get more biomass for the measurements. The influence of a higher biomass on the reduction process was determined in advance and no major differences occurred (see Fig S4). Due to the low biomass used in the experiments compared to the relatively high sample volumes required for the X-ray absorption spectroscopic measurements, larger volumes of uranium-incubated cell suspension were employed for these experiments. Overall, 250 mL of the U(VI)-incubated cell suspensions (quintuplets of 50 mL in 100-mL serum bottles) were used per time point containing a DBM of 22 mg cells (4×10^7 cells). Incubation took place in quintuplicates containing 50 mL cell suspension each. The expected removal of uranium in the supernatants was proven by measurement of the uranium concentrations in each sample via ICP-MS. Cell pellets were collected after certain incubation times by centrifugation at 10.000 x g at 18 °C for 10 min gathered in a single sample vial and washed with artificial Opalinus Clay pore water solution. Afterwards, for EXAFS measurements, the cell pellet was transferred as wet paste in a 3-mm-thick polyethylene sample holder double-confined with 13 micron Kapton tape and polyethylene. For HERFD-XANES measurements, the cell pellet was transferred into a sample carrier with round recess of 1 mm depth single-confined with 13 micron Kapton tape only, to allow low-energy M_4 edge X-ray beams to reach the sample. The uranium M_4 HERFD-

XANES measurements[50,51,64] and the uranium L_3 transmission EXAFS measurements[65] were performed at beamline BM20[66] at the European Synchrotron Radiation Facility (ESRF) in Grenoble. For XANES measurements, the incident energy was selected using the 111 reflection from a double Si crystal monochromator. XANES spectra were measured in high-energy-resolution fluorescence-detected (HERFD) mode using an X-ray emission spectrometer.[67] The sample, analyzer crystal, and photon detector (silicon drift detector) were arranged in a vertical Rowland geometry. The uranium HERFD spectra at the M_4 edge were obtained by recording the maximum intensity of the uranium M_b emission line (~3337 eV) as a function of the incident energy. The emission energy was selected using the 220 reflection of five spherically bent striped Si crystal analyzers (with 0.5-m bending radius) aligned at 75° Bragg angle. The intensity was normalized to the incident flux. The paths of the incident and emitted X-rays through air were minimized in order to avoid losses in intensity due to absorption. Data was collected under cryo conditions with cryostream on a sample. All samples have been tested for short-term beam damage, since in some cases, X-ray may induce the reduction of many elements. First, an extended time scan (>2 min with 0.1 s exposure time per step) at the maximum of the U M_4 edge white line was performed before data collection, to monitor any long-term variations in the fluorescence signal. Later several fast HERFD scans (total counting time is less than 10 s) in the short energy range were performed and compared with all HERFD data collected per sample. Based on that procedure, the estimated X-ray exposure time can be derived for each sample. However, we didn't find any evidence of the spectral change caused by X-ray exposure.

EXAFS measurements were performed as previously described,[60] but under cryogenic conditions (15 K by using a closed-cycled He-cryostat). The ionization potential at the uranium L_3 edge was set arbitrarily to 17185 eV. EXAFSPAK was used for the data treatment such as energy calibration, averaging of multiple sample scans, correction for the X-ray absorbing background, isolation of the EXAFS signal, and the shell fit.[68] The ab-initio scattering code FEFF8.20[69] was used for the calculation of the scattering phase- and amplitude functions based on a structural model of a trimeric U(VI)-tartrate complex and a modified structure of the mineral ningyoite (Figs S17, S18).[70] Assuming the presence of coexisting U(IV), U(V), and U(VI) species, iterative target transformation factor analysis (ITFA)[71] was applied for the mathematical decomposition of the originating spectral mixtures into the spectra of the pure uranium species, i.e. components, and their fractions

in HERFD-XANES and EXAFS data. Furthermore, target factor analysis (TFA)[60,72,73] was applied for the chemical identification of the uranium species by using 81 EXAFS reference spectra from various organic and inorganic chemical systems with uranium in the oxidation states IV, V, and VI (Figs S19, S20).

3 Results & discussion

3.1 Uranium concentration in the supernatants

A time-dependent U(VI) reduction experiment in artificial Opalinus Clay pore water was performed to find out whether *D. hippei* DSM 8344^T is capable of reducing U(VI). Two different initial concentrations of 100 and 500 µM U(VI) were used to investigate the occurring processes. Fig 1 shows the concentration of uranium in the supernatants in dependence on the incubation time.

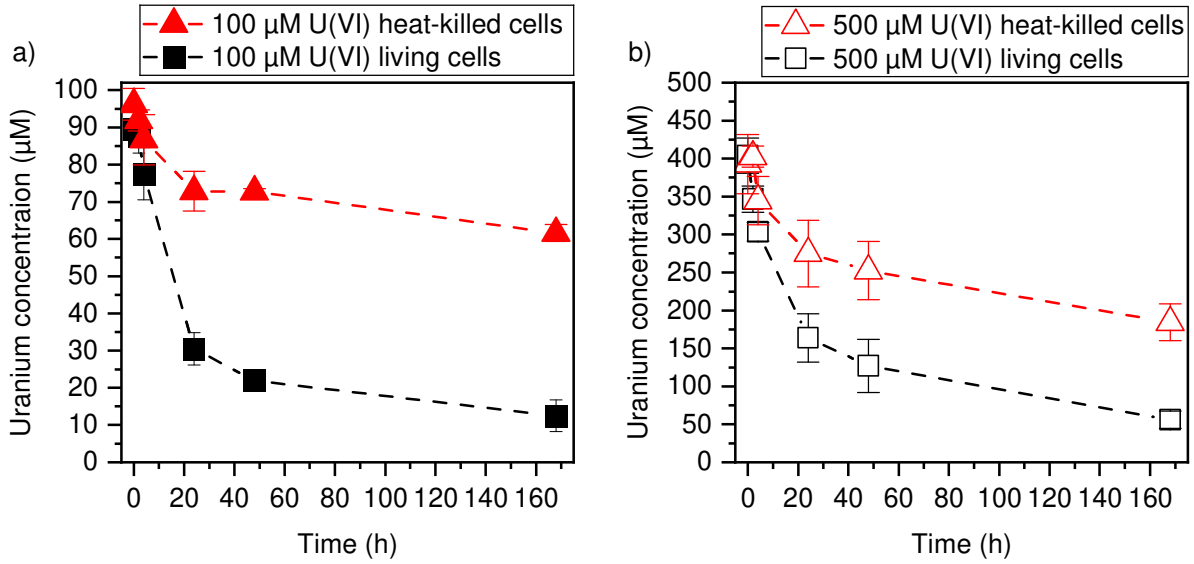

Fig 1. Uranium concentration in the supernatants of the batch experiments with living and heat-killed cells of *D. hippei* DSM 8344^T with an initial U(VI) concentration of a) 100 µM and b) 500 µM (artificial Opalinus Clay pore water, pH 5.5, 10 mM lactate, DBM = 0.044 mg/mL, 8x10^5 cells/mL).

A decrease in uranium concentration in the supernatants of the experiments with living cells is visible with increasing incubation times for both concentrations. At the lower U(VI) concentration of 100 µM, within 48 h, around 80% of the uranium were removed from the supernatants, after one week almost 90%. The reduction experiment with 500 µM U(VI) also showed an almost complete removal of the uranium from the supernatants. Within 4 h, 40% were already removed, and after one week, only 10% of the initial

uranium was still detectable. At both concentrations, black-brown precipitates occurred after certain incubation times, suggesting the reduction of soluble U(VI) (Fig S5). Stability of the pH values of the samples during the experiment were checked for the initial U(VI) concentration of 100 µM (Fig S6). A comparison with other *Desulfosporosinus* spp. shows a similar, only slightly faster removal of uranium from the supernatants. In case of the strains P3 and DSM 765, the process is almost completed after 24 h at a slightly higher pH value of 7, 1 mM uranyl(VI) acetate, and 1 mM lactate.[23,24] However, similar time frames for the uranium removal were also observed by iron-reducers as *Geobacter* spp. and *Shewanella* spp.[14,33,74] Furthermore, experiments with heat-killed cells were performed. At 100 µM U(VI), 35% of the uranium was removed from the supernatant after one week, probably due to different association processes, *e.g*. biosorption to functional groups on the cell surface.[5] The heat treatment promotes cell breakup, which provides more binding sites for uranium association. Therefore, dead cells generally bind more uranium in contrast to living cells.[75,76] In addition, it could be that the heat treatment did not completely kill all the cells. In this case, the surviving cells can contribute to the decrease of the uranium concentration in the supernatant. However, the removal of U is significantly higher in the living cell experiment compared to the experiment with the heat-killed cells. Therefore, the living cells contribute through their activity to the higher removal of uranium in the living-cell experiments. The experiment with heat-killed cells at the higher initial U(VI) concentration shows a relatively high removal of uranium from the supernatants. However, the proportion of the removed uranium is still not as high as in the experiment with the living cells. In this case, a partial precipitation of U(VI) during the experiment due to the higher initial concentration could also contribute to the increased values of U removal from the supernatants.

For further investigation of the occurring processes, lactate and sulfate concentrations were determined during the bioreduction experiments (Fig S7). The initial sulfate concentration in Opalinus Clay pore water solution is about 14 mM. Until 48 h, the sulfate concentration remains almost constant. Only after one week, a slight decrease is observed, probably due to a reduced bioavailability of the U(VI). Therefore, this microorganism seems to reduce U(VI) prior to sulfate. These results are also in good agreement with the redox potentials of both ions (pH 7: $E(UO_2^{2+}/U^{4+}) = 0.12$ V, $E(S^{2-}/SO_4^{2-}) = -0.2$ V).[77,78] The higher reduction rate of sulfate in the experiment with 500 µM U(VI) (Fig S7) could be due to an increased co-precipitation of U(VI) and U(IV). In this case, the bioavailability of U(VI)

would decrease, which would favor sulfate reduction. Furthermore, no decrease in sulfate concentrations was detected in the heat-killed-cell experiment.

With help of HPLC measurements, changes in the lactate concentration over time were determined (see Fig S7b). Lactate can serve as an electron donor for the reduction of U(VI) and is itself oxidized to acetate. Therefore, lactate concentrations should decrease over time. Evaluation of the HPLC data indicates a decrease, but only small amounts of the lactate are consumed. A reason for this could be the huge excess of lactate in the samples in comparison to the proportions of uranium. Furthermore, for every molecule of lactate, which is oxidized, two uranyl(VI) ions can be reduced according to stoichiometry. The formation of acetate could also be determined via this method. An acetate peak was visible via HPLC measurements, but the amount was too low to be quantified.

U(VI) reduction experiments under anaerobic conditions are often performed in a bicarbonate-buffered medium to stabilize U(VI) in solution.[14,16–18,25,26,33] *D. hippei* DSM 8344^T was also investigated regarding its capability of reducing U(VI) in 30 mM bicarbonate buffer in the presence of lactate (Fig S8). In this case, no dark precipitates and no decrease in uranium concentration in the supernatants occurred. Therefore, we assume that *D. hippei* DSM 8344^T cannot reduce U(VI) in bicarbonate buffer, where the 1:3-uranyl(VI)-carbonate complex is the dominant species (Fig S9a). This is also in good agreement with former findings of Suzuki *et al*., who investigated the reduction of U(VI) by other *Desulfosporosinus* spp.[24] These strains were also not capable of reducing U(VI) in the presence of bicarbonate. The present uranyl(VI)-carbonate complex apparently cannot be reduced by this bacterial genus. Potential explanations could be, as already determined by Suzuki *et al*., that these microorganisms do not contain *c*-type cytochromes [13], which seems to play an important role for the U(VI) reduction by other bacteria.[19,28] In addition, it was described that some *Desulfosporosinus* spp. can grow using bicarbonate as the sole electron acceptor in combination with lactate as an electron donor during homoacetogenic fermentation.[79] In this case, this energy metabolism would be preferred by the microorganisms, because the microorganisms will gain more energy by this metabolism.

3.2 Fluorescence spectroscopic studies of the supernatants

To get more information about the U(VI) speciation in the supernatants, time-resolved laser-induced fluorescence spectra were recorded at different time points of the batch

experiment. The U(VI) emission spectra of the supernatants after different times of incubation with cells of the anaerobic bacterium *D. hippei* DSM 8344^T are shown in Fig 2a.

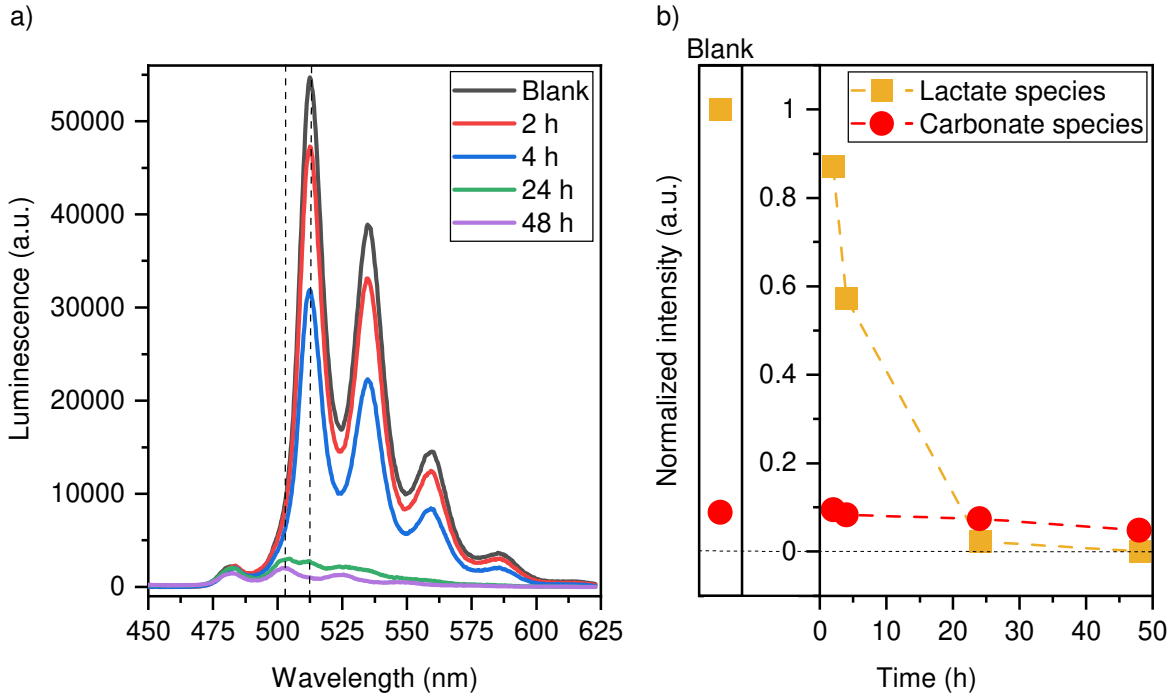

Fig 2. a) Emission spectra of the supernatants after different incubation times (2 h – 48 h) with *Desulfosporosinus hippei* DSM 8344^T in artificial Opalinus Clay pore water ([U(VI)$_{initial}$] = 100 µM; [Lactate] = 10 mM; excitation wavelength = 266 nm); b) distribution of the U(VI) species in the supernatants as a function of the incubation time determined by parallel factor analysis (PARAFAC)[80] (orange = uranyl(VI)-lactate complex, red = 1:1-uranyl(VI)-carbonate complex).

The experiment was performed in artificial Opalinus Clay pore water with an initial U(VI) concentration of 100 µM. Already the initial spectra show a decrease in the luminescence intensity with time, which is in good agreement with the decreasing U(VI) concentrations in the samples. Overall, two species occur in the spectra, with both species showing approximately the same intensity after 24 h (Fig. 2a). Furthermore, there is no significant difference between the blank spectrum of the initial U(VI) solution and the spectra after up to 4 hours. Prior to the exposure of cells, the speciation of U(VI) in artificial Opalinus Clay pore water with 10 mM sodium lactate was modeled, and a uranyl(VI)-lactate complex was found to be the dominant species under these conditions (pH 5.5). Furthermore, a uranyl(VI)-carbonate complex was determined to a lesser extent. The results of this modeling can be found in the supporting information (Fig S9b, c) and provide insights into the U(VI) speciation in the supernatants for the initial solution (blank).

It is not possible to draw direct conclusions from the emission spectra about the different involved U(VI) species in the supernatants, because of the partial superposition of the single-component spectra. Therefore, a deconvolution of the spectra with the help of the mathematical method called parallel factor analysis (PARAFAC) was carried out.[80] The spectra of two different species could be extracted in this way (Fig S10), which is already in good agreement with the previous calculations. With the help of several reference spectra from previously determined species, an assignment to two different uranyl(VI) compounds was possible. The band positions of the extracted spectra and references are shown in Table 1. The first extracted spectrum shows a high agreement with a uranyl(VI)-lactate complex. The reference was prepared and measured under the same conditions as the samples. Both, spectral decomposition and band positions are in good agreement. The formation of this complex is favored at a pH of 5.5 because of the high excess of lactate in the samples. The second spectrum also shows a very good agreement with the reference of the 1:1-uranyl-carbonate complex originating from sodium bicarbonate in the Opalinus clay pore water solution and the gasification with a mixture of 20% carbon dioxide and 80% nitrogen to get the solutions anaerobic. All in all, both calculated species could be confirmed experimentally with luminescence spectroscopy.

Table 1. Assignment of the band positions of the extracted time-resolved laser-induced fluorescence spectra (Fig S10). Extraction of the spectra was performed using PARAFAC[80].

	Band position (nm)					Reference
Spectrum 1	512.5	534.7	559.4	585.7	614.6	This work
Uranyl(VI)-lactate	511.8	534.0	558.1	584.9	614.0	This work
Spectrum 2	482.3	503.3	524.5	547.9	575.0	This work
UO_2CO_3	482.0	502.9	525.6	549.2	575.1	[58]

The species distribution (Fig 2b) shows that the uranyl(VI)-lactate species is the major component in the initial solution. During the reduction process, the species distribution shows a decrease of the uranyl(VI)-lactate species with time. In contrast to this, the proportion of the carbonate complex remains almost constant. This can be attributed to the assumption that this genus cannot reduce the uranyl(VI)-carbonate species.[24] This would be in good agreement with the non-changing values of U(VI) concentrations in the supernatants of the bicarbonate experiment and shows the influence of the initial U(VI) species on U(VI) reduction by this microorganism.

In addition to these results, a luminescence spectroscopic experiment with more frequent sampling showed an interesting behavior of the luminescence intensities over time, especially during the first hours of the bioreduction process. Although the emission intensity of uranyl(VI) underwent a general decrease, the rate of this decline is not consistent (Fig S11). Instead, the luminescence intensities decrease and increase several times. An initially sharp decrease of the intensity is followed by a subsequently partial increase. This distinctive 'saw tooth' pattern was already observed in other bioreduction processes, *e.g.* in the reduction of U(VI) by *Geobacter sulfurreducens* and *Shewanella oneidensis*.[7,33] These studies explained the observed pattern by the formation of uranyl(V) as an intermediate uranium species during the reduction. Therefore, time-resolved luminescence spectroscopy could give an indication of the occurrence of U(V) during reduction by sulfate-reducing microorganisms.

3.3 Microscopic investigations

Live/dead staining of the cells was carried out at different incubation times. The images show an increased agglomeration of the cells with the incubation time at both concentrations (see Fig S12). In addition, the proportion of the dead cells increases, what becomes clear from the yellowish color of the agglomerates indicating a mixture of living (green) and dead (red) cells. In contrast to this, those agglomerates do not occur in the cell blank without U(VI) incubation, not even after one week. The live/dead images at both concentrations do not differ significantly from each other. At the higher U(VI) concentration of 500 µM, the agglomerates are slightly bigger than those in the experiment with an initial U(VI) concentration of 100 µM.

The localization of uranium in/on the cells was investigated by scanning transmission electron microscopy (STEM) analyses of ultrathin sectioned samples of the U(VI)-incubated cells. In particular, atomic-number-contrast HAADF-STEM imaging was combined with spectrum imaging analysis based on energy-dispersive X-ray spectroscopy (EDXS). Fig 3 shows the resulting images and U distribution maps for two U(VI) concentrations (100 µM and 500 µM) and two incubation times (4 h and 24 h).

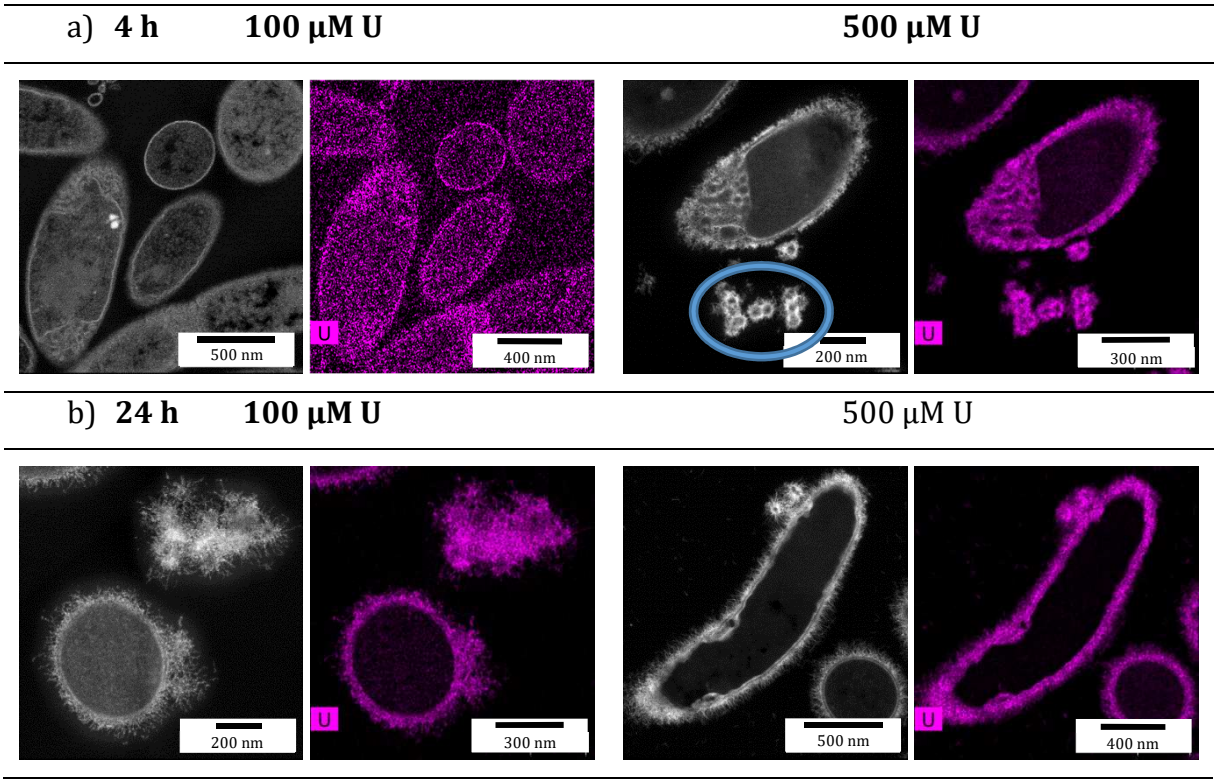

Fig 3. Representative HAADF-STEM images (left) and corresponding U element distribution (right) of ultrathin sectioned samples of *Desulfosporosinus hippei* DSM 8344^T cells treated with uranium ([U(VI)$_{initial}$] = 100/500 µM) for a) 4 h and b) 24 h. The blue ellipse highlights possibly released membrane vesicles.

The amount of cell-associated uranium increases with time and concentration, which is in good agreement with the decreasing uranium concentrations in the supernatants (see Fig 1). Uranium-containing aggregates are mainly present on the cell surface. These partly have the shape of small needles (for higher magnification see Fig S13). High-resolution TEM imaging coupled with fast Fourier transform analysis for *D. hippei* DSM 8344^T after incubation with 500 µM U(VI) for 24 h showed the aggregates to be of amorphous structure (Fig S14). Especially at the lower concentration and with shorter incubation times, uranium is located also inside the cells, almost evenly spread (Fig 3a). As can be seen in the images (blue ellipse, Fig 3a), there is an indication for the release of membrane vesicles from the cell surface. This could be a possible defense mechanism of *D. hippei* DSM 8344^T to mitigate cell encrustation and has already been reported for other microorganisms, *e.g. Shewanella oneidensis* MR-1 or *Geobacter sulfurreducens*.[81,82]

3.4 UV/Vis spectroscopy

The formation of U(IV) was proven by UV/Vis studies of the dissolved cell pellets. Fig 4a shows the UV/Vis spectra of the dissolved cell pellets after different incubation times in comparison with the reference spectra of U(VI) and U(IV).

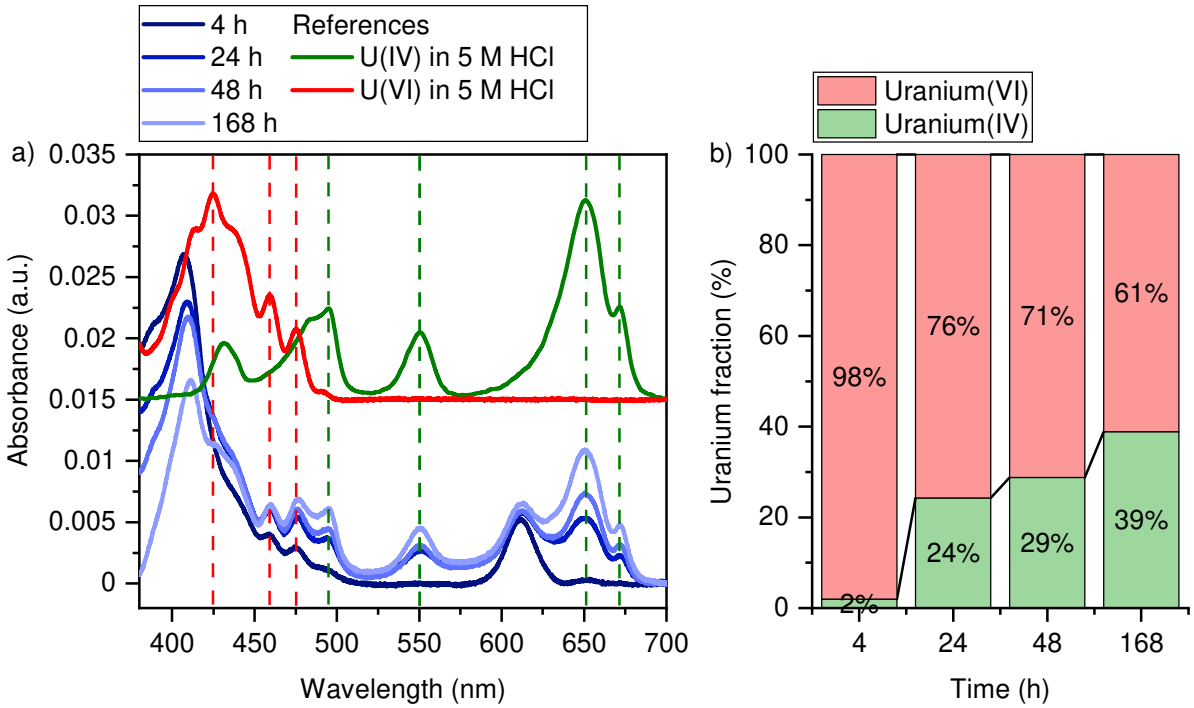

Fig 4. a) UV/Vis spectra of the dissolved cell pellets after different incubation times in comparison with normalized reference spectra of U(IV) and U(VI). b) Calculated proportions (see supporting information) of U(IV) and U(VI) under consideration of the corresponding extinction coefficients of both oxidation states ($[U(VI)_{initial}]$ = 100 µM).

A comparison of the band positions provides clear proof of the formed U(IV). At the characteristic band at around 650 nm, we observe an increase in the proportion of U(IV) with time, which becomes visible in the spectra. In the spectral region between 400 and 500 nm, also bands of U(VI) are still detectable. These partly overlap with those of U(IV). This suggests that not all of the U(VI) is reduced to the lower oxidation state in the cell pellets, and therefore the fraction of removed uranium from the supernatants is not entirely U(IV), not even after one week. Consequently, the occurring process seems to be based on a combination of association with the cells and reduction. The band at a wavelength of 610 nm is caused by residual cell components, because a blank spectrum of a dissolved cell pellet without U(VI) incubation also shows this feature (Fig S15). The band at 410 nm, which partly overlaps with bands of U(VI), can provide further indication of intermediately occurring U(V) during the reduction process, which disproportionates to U(VI) and U(IV). Nagai *et al*. investigated the absorption properties of U(V) in molten

NaCl-2CsCl.[83] They showed that U(V) exhibit an intense absorption band at this wavelength. Further data evaluation regarding this oxidation state were not performed because of the huge differences in the chemical surroundings, affecting different physical quantities, *e.g*. the molar attenuation coefficient. It would be possible, however, that the proportion of U(VI) in the samples is lower, since the proportion of the possibly occurring U(V) would have to be subtracted. Therefore, to get the exact values of the proportions of U(VI) and U(IV) in the cell pellets at every time point, calculations considering the molar extinction coefficients were carried out.

As can be seen in Fig 4b, the proportion of U(IV) in the samples increases continuously with time. After 4 h, only a very small proportion of the U(VI) is reduced. Only 2% of U(IV) are present in the samples. But already after 24 h, round about a quarter of the U(VI) is reduced to U(IV) in the cell pellets. This value is further increasing until one week, where about 40% are reduced. However, when comparing the percentages of the different oxidation states over time, the different proportions of cell-associated uranium must also be taken into account. Especially after 4 h, only 20% of the uranium are removed from the supernatant. After 24 h, however, the proportions do not change much. The UV/Vis experiment with heat-killed cells only shows a minor reduction of U(VI) under these conditions (Fig S15). This can be due to a partly reduction, possibly caused by remaining living cells after heat treatment or by a light-mediated reaction with lactate[84,85] . However, the intensity of the uranium(IV) band at 650 nm is much weaker than in the experiment with the living cells. Furthermore, no differences in the reduction behavior could be observed in the experiments with incubation in the dark (data not shown). Therefore, reduction of U(VI) by lactate seems to have only a minor or no influence on the experiments.

3.5 High-energy-resolution fluorescence-detected X-ray absorption near-edge structure spectroscopy (HERFD-XANES)

The electronic structure of the uranium system has been investigated by HERFD-XANES measured at the uranium M_4 edge, which probes directly the f-orbitals through $3d_{3/2} \rightarrow 5f_{5/2}$ electronic transitions.[50,51,64] The appearance of the main HERFD transitions at different incident energy in the X-ray spectroscopy process is generally attributed to the change of the oxidation state, which produce the chemical shift of the detected 3d-5f tran-

sitions.[50] Fig 5 shows the HERFD-XANES spectra of the cell pellets after different incubation times in comparison with the reference spectra of U(VI), U(V),[86] and U(IV). Reference spectra for U(VI) and U(IV) were measured simultaneously with the samples.

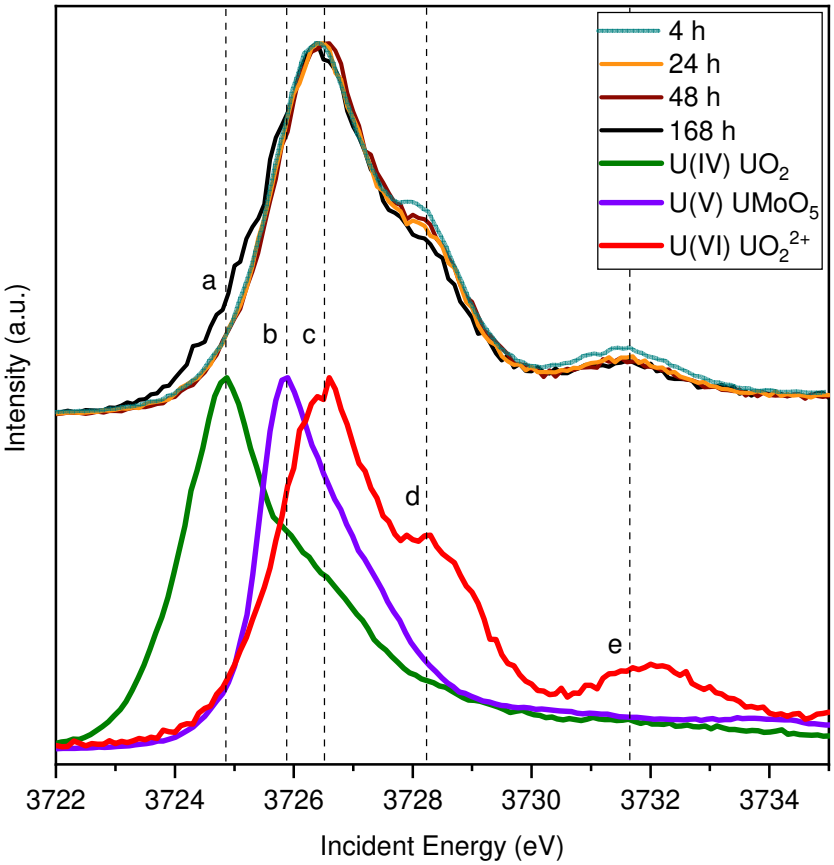

Fig 5. Uranium M_4 HERFD XANES data recorded on the cell pellets after different incubation times compared with the reference spectra of U(VI) as uranyl(VI) nitrate, U(V) as $UMoO_5$,[86] and U(IV) as UO_2. Dashed lines in a–c indicate the white line energy positions for U(IV), U(V), and U(VI) valence states, respectively; d and e indicate post-edge feature for the uranyl(VI) structure ($[U(VI)_{initial}]$ = 100 µM).

Figure 5 shows that spectra recorded on cell pellets after the 4 h, 24 h, 48 h, and 168 h incubation time are different. First of all, the intensity of the first post-edge feature (marked d) after the white line (marked c) is gradually going down upon increasing incubation times. The second post-edge feature (marked e) has the same tendency. Generally, the hexavalent uranium M_4 HERFD shows three features (marked c, d, e)[51] and reflect the f density of states for the specific atomic orbital. Data recorded on cell pellets after different incubation times show that U(VI) is the dominant uranium oxidation state for all samples, but some tiny differences, as explained above, are still noticeable. Moreover, the uranium spectrum recorded for a sample with 168 h incubation time is much broader

than other spectra and there is also a shoulder on the left side from the main edge transitions. The appearance of the shoulder at the low-energy side is generally attributed to the formation of lower oxidation states – the formation of the U(IV) or/and U(V). In order to extract the exact contributions of U(IV), U(V), and U(VI), we used the ITFA package.[71] As input files, we used the UO_2 as U(IV), the uranyl(VI) as U(VI), and U(V) has been taken as uranate in $UMoO_5$ published by Pan *et al*.[86] ITFA-extracted eigenvectors of the HERFD-XANES data, isolated single-component spectra and the reproduced U M_4 HERFD spectra, as well as differences between experimental and reproduced spectra are shown in Fig S16. The results of the ITFA analysis are presented in Table 2 and provide first evidence of the presence of U(V) in the microbial reduction not only by the non-cytochrome-c containing bacteria *D. hippei* DSM 8344^T, but also by sulfate-reducing bacteria in general. The proportion of this oxidation state remains almost constant over the investigated time frame, which indicates a stabilization by the chemical surrounding as previously described.[37–49] Furthermore, these findings verify the above-mentioned indications of this oxidation state via UV/Vis and luminescence spectroscopy.

Table 2. Fractions of U(VI), U(V), and U(IV) calculated by ITFA analysis.[71] Estimated error of the ITFA analysis is 2%.

Time (h)	U(VI) (%)	U(V) (%)	U(IV) (%)
4	74	25	1
24	67	31	2
48	72	27	1
168	60	30	10

We noticed that the estimated amount of different oxidation states from HERFD data is different from those extracted from UV/Vis. For example, for the 4h sample the U(VI) contribution was found to be 98% from UV/Vis versus 74% by HERFD. It can be related to the fact that in the UV/Vis experiments, the whole cell pellet is dissolved and measured, whereas in the HERFD-XANES studies, only a small spot of the sample is analyzed due to the limited dimension of the X-ray beam.[66] Nevertheless, the overall tendency of the U(IV) oxidation state over different incubation times is similar for UV/Vis and HERFD. In contrast to the iron-reducing microorganisms *Shewanella* and *Geobacter*, U(VI) reduction proceeds much more slowly in *D. hippei* DSM 8344^T.[33,34] In case of *Shewanella oneidensis*, after 4.5 h, already 24–25% of the uranium was reduced to U(IV) in the cell pellets and

after 120 h, the proportion of U(IV) was approx. three quarters. Furthermore, also the proportion of U(V) during the reduction is higher for *Shewanella*. However, the pentavalent oxidation state persists for longer incubation times in the reduction experiments with both microorganisms.[33] For *Geobacter*, the reduction process is even faster as determined by L_3-Edge EXAFS spectroscopy. In this case, after 24 h, all the uranium has been reduced to U(IV) and U(V) only occurs in samples after 4 h of incubation.[34]

3.6 Extended X-ray absorption fine structure (EXAFS)

In order to estimate the number (n) and fractions of the coexisting uranium species and to isolate their spectra from the spectral mixtures, the EXAFS spectra of four samples at incubation times t = 4 h, 24 h, 48 h, and 168 h were analyzed with ITFA and TFA. As shown in Fig 6 the linear combinations of the ITFA-calculated first two eigenvectors reproduce the experimental spectra in high quality, hence only two spectral components are present and change their fractions as a function of the incubation time, thus determining the shape of the spectral mixtures.

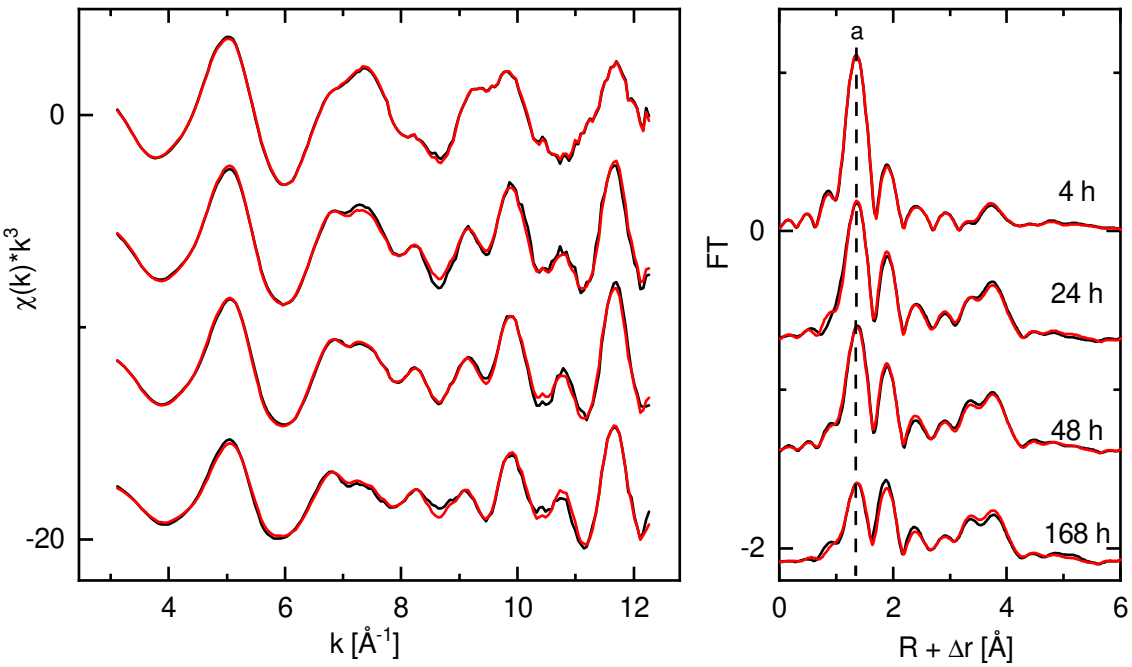

Fig 6. Experimental (black) and ITFA-reproduced (red) uranium L_3 EXAFS spectra recorded on the cell pellets of *D. hippei* DSM8344^T after incubation with uranium [100 µm] for different times (left) with corresponding Fourier transforms (FT) (right). FT peak of the axial oxygen atoms (a).

In a first attempt, the chemical origin of the two spectral components can be deduced by the inspection of the Fourier transform (FT) of the spectral mixtures. The systematic decrease of the FT peak at 1.36 Å, coming from the axial oxygen atoms (O_{ax}) of the U(VI) "yl" unit (Fig 6a)), points to an increase of the fraction of U(IV) with increasing incubation time, because for U(IV) no O_{ax} peak is expected in the FT. However, at the highest incubation time, there is still a significant fraction of the U(VI) species present, as visible at the O_{ax} FT peak (Fig 6, t = 168 h), so that the U(IV) species does not provide its pure experimental spectrum in the series. This is in good agreement with the UV/Vis and HERD-XANES data. Consequently, the spectral mixtures have to be mathematically decomposed so that the resulting spectra of the pure uranium species can be analyzed by the shell fitting approach. For the calculation of the fractions and spectra of the uranium species, ITFA needs at least n^2-n known fractions (n = number of spectral components) as constrains, hence two known fractions in the present case. However, only for the U(VI) species, we can assume 100% at t = 4 h, while no data are available for the U(IV) species. Fortunately, the fact that the O_{ax} signal can serve as an unequivocal and robust measure of the presence of U(VI) and that the fractions of a component can be calculated independently to the fractions of the remaining components by ITFA owes the possibility to calculate and isolate the fractions and spectra of the pure uranium species by a simple minimization strategy applied on the O_{ax} FT peak (see SI). As shown in Fig 7 and in comparison with the spectrum at t = 168 h (Fig 6), the O_{ax} FT peak vanishes substantially for the U(IV) species after the proposed ITFA treatment so that both isolated spectra refer to uranium species in their pure oxidation states for which a shell fit can be performed. The resulting fractions (Table 3) deviate strongly from those observed by the HERFD measurements (Table 2) where U(V) was detected in addition to U(IV) and U(VI). However, the penetration depth of the X-rays at the U M_4 and at the U L_3 edge is different, which variates slightly the obtained results at the U L_3 or U M_4 edges. In addition, a lack of U(V) references for EXAFS, as well as the structural similarity of U(VI) and U(V), making it difficult to assign the isolated spectra to this oxidation state.

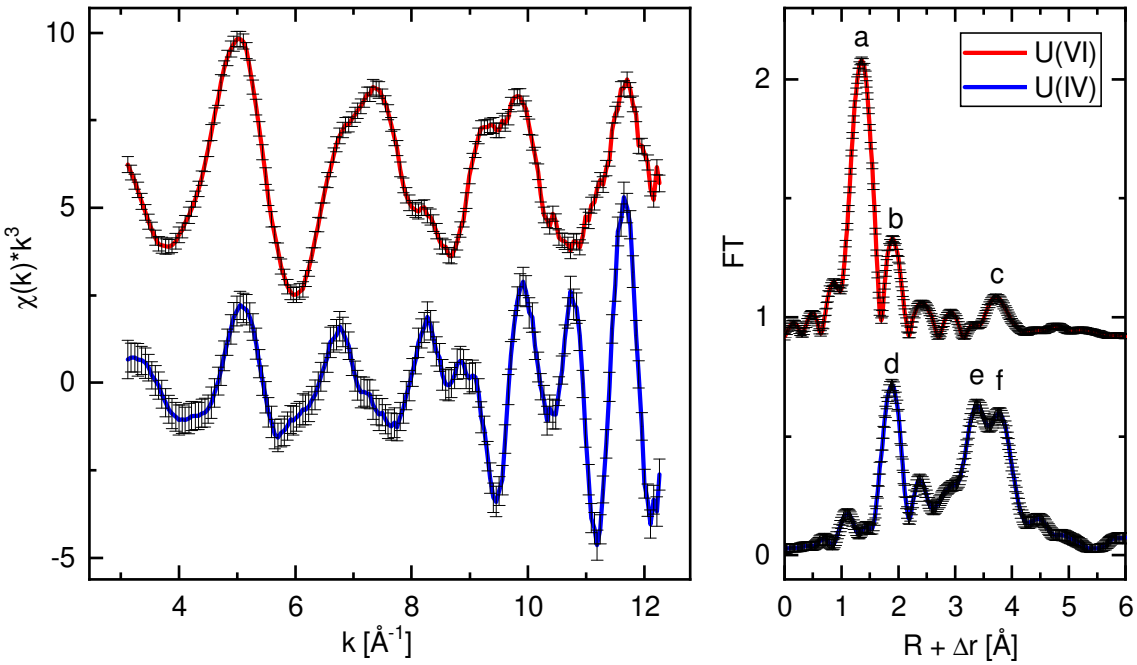

Fig 7. Uranium L_3 EXAFS spectra of the ITFA-isolated spectra of the isolated uranium species (left) with corresponding Fourier transforms (FT) (right) and estimated standard deviations (black). FT peaks of the axial oxygen (O_{ax}) (a), equatorial oxygen (O_{eq}) of U(VI) (b), first oxygen shell of U(IV) (d), and uranium interactions (c, e, f).

Table 3. Fractions of U(VI) and U(IV) calculated by ITFA analysis (see SI).

Time (h)	U(VI) (%)	U(IV) (%)
4	100	0*
24	62(1)	38(1)
48	57(1)	43(1)
168	55(2)	45(2)

* - fixed during ITFA procedure. Estimated standard deviations in parenthesis.

TFA can be used to identify spectra from different chemical reference systems whose linear combinations are suitable for the reproduction of spectral mixtures. Thus, TFA allows the chemical identification of the uranium species. For this purpose, each reference spectrum (target) is subjected subsequently to the TFA procedure, while the SPOIL value[87] measures for each target its suitability for the reproduction of the spectral mixtures. As lower the SPOIL value as higher the probability that the subjected target spectrum refers to a pure chemical species contained in the spectral mixtures. Here, we used about 81 EXAFS spectra from U(IV), U(V), and U(VI) systems with different inorganic and organic

ligands at various pH, concentrations, and temperatures (Figs S19, S20). Notably, if we exclude the formation of schoepite measured at room temperature (SPOIL = 2.25) and at 15 K (SPOIL = 2.58), then only reference spectra of U(VI) with exclusively aqueous hydroxy-carboxylic acids like lactate, tartrate, citrate, and malate form two groups of possible references measured at room temperature (RT). In the first group, all acids between $6.6 \leq pH \leq 7$ with $1.78 \leq SPOIL \leq 2.22$ are contained, while the second group consists of tartrate and lactate with SPOIL = 2.71 and 2.78 at pH 5.0 and 5.5, respectively. Moreover, from a chemical point of view in the lower pH range, significant portions of polynuclear dimeric and in the higher pH range, dominating trimeric U(VI) complexes are expected for these hydroxyl-carboxylic acids.[88–92] However, U(VI) with lactate at pH 7 is the reference with the lowest SPOIL value of 1.78, hence the most probable U(VI) species in the system. In the case of the other oxidation states, the spectra with the lowest SPOIL value corresponds to colloidal $U(IV)O_2$ (SPOIL = 3.9) and U(V)-carbonate (SPOIL 13.9), respectively. Hence, both can be considered already as non-matching references. The shell fit of the best matching reference (U(VI) with lactate, pH 7) and of the ITFA-isolated spectra (Fig 7) is shown in Fig S21, while the EXAFS structural parameter are summarized in Table 4. In the case of the U(VI) species, the radial O_{ax} distance (R_{Oax}) matches R_{Oax} obtained for U(VI)-lactate, while the radial distance of the equatorial (eq) oxygen atoms (R_{Oeq}) is by 0.04 Å less, a value which exceeds the common absolute error in determination of EXAFS radial distances of ±0.02 Å.[93] Due to the vanishing thermally induced atomic disorder, a decrease of the Debye-Waller factor (DW) is expected for measurements at low temperatures,[94] thus we assumed for the U-U interaction a DW of 0.006 $Å^2$ and of 0.003 $Å^2$ for U(VI)-lactate and for the U(VI)/U(IV) species measured at RT and 15 K, respectively. The fit of the uranium shell reveals a coordination number (CN) of one at 3.88 Å and two at 3.83 Å for the U(VI) species and the U(VI)-lactate, respectively. Together with the common error in determination of CN of about 20%,[93] the gained structural parameter (R, CN) deviates between the two spectra. However, these deviations are still relatively small, as visible in the overall agreement between the two spectra (Fig S21a and b). Note that especially for trimeric U(VI) species, the uranium core can be structurally different due to the presence or absence of a uranium-connecting central μ_3-O atom[95–98] (Fig S17), which can lead to slight differences in the EXAFS structural parameter between the two isomeric forms. Furthermore, TFA yields from 81 chemically relevant systems the most probable references which are also the most reasonable from a chemical point of

view so that we conclude, together with the results of the luminescence spectroscopic studies (see above) the presence of a dimeric or trimeric U(VI)-lactate complex in the system.

In the case of the U(IV) species, the first shell oxygen peak is strongly reduced (Fig 7d) pointing to a strong structural disorder which deteriorates the shell fit if only one oxygen shell is included. Thus, the first shell needs to be split into at least two shells with R_{O1} = 2.36 Å and R_{O2} = 2.61 Å, while for the fit, the total sum of their CNs are kept at CN = 8, which was recently assumed for biogenic formed U(IV) species.[99,100] A carbon shell with R_c = 2.89 Å is needed to reach a proper quality of the fit, while a phosphate group at 3.06 Å can be ruled out as proved by an F-test according to Downward *et al*. (see supporting information)[101] Two uranium interactions (two up to three U at 3.65 Å and at 3.87 Å) yield a good description of the degenerated peak between 3.0-4.3 Å in the FT (Fig S21c)). This double peak in the Fourier transform differs significantly from other U(IV) compounds (Fig S19). According to the TFA analysis, no reference spectrum matches the U(IV) species and any attempts of fitting using a uraninite- or a ningyoite-like biogenic phosphate structure[100] proved unsuccessful. Since these end products of uranium reduction by several environmentally relevant bacteria (Gram-positive and Gram-negative) and their spores can include a variety of U(IV) species, *e.g*. different phosphate compounds, various phosphate references also showed no agreement with the recorded spectra (Fig S19).[25,26] However, in comparison to different other studies characterizing the biogenic products of the U(VI) reduction as UO_2,[24,30–32] or ningyoite-like phosphates[100] in our study, another structure is formed. Furthermore, we cannot exclude that the isolated U(IV) spectrum consists of the sum of signals coming from multiple structurally different U(IV) species. In the special case, these species does not change their fractional ratios in the time series. Thus, we can give for the U(IV) species no reliable structural explanation at the moment.

Table 4. EXAFS shell fit structural parameter obtained for the best matching reference spectrum (U(VI)-lactate[92]) and for the isolated spectra of the U(VI) and U(IV) species.

Path/sample	CN	r/Å	σ^2/Å^2	ΔE_0/eV
U(VI) with lactate at pH 7 at RT ([U] = 50mM, [lactate] = 0.5 M)				
U–O_{ax}	2*	1.795(1)	0.0017(1)	4.0(3)
MS$_{Oax}$	2/	3.590/	0.0034/	4.0/
U–O_{eq}	5*	2.358(5)	0.0147(5)	4.0/
U–U	2.1(1)	3.826(4)	0.006*	4.0/
U(VI) species at 15 K				
U–O_{ax}	2*	1.796(2)	0.0020(1)	3.7(4)
MS$_{Oax}$	2/	3.592/	0.0040/	3.7/
U–O_{eq}	5*	2.321(6)	0.0191(8)	3.7/
U–U	0.95(8)	3.876(4)	0.003*	3.7/
U(IV) species at 15 K				
U-O_1	4.8(2)	2.360(3)	0.0054(4)	4.9(6)
U-O_2	3.2+	2.610(1)	0.0074/	4.9/
U-C	3.5(3)	2.891(7)	0.004*	4.9/
U-U_1	2.5(2)	3.648(4)	0.003*	4.9/
U-U_2	3.3(2)	3.870(4)	0.003*	4.9/

CN – coordination number, r – radial distance, σ^2 – Debye-Waller factor, ΔE_0 - shift in energy threshold. Parameter fixed (*), linked (/), and linked to keep constant sum (+). Estimated standard deviations of the variable parameter as given from EXAFSPAK in parenthesis. Amplitude reduction factor (S_0^2) was set to S_0^2 = 0.9. In the case of U(VI) the twofold degenerated 4-legged multiple scattering (MS_{Oax}) path, U-$O_{ax(1)}$-U-$O_{ax(2)}$-U, was included in the fit.

4 Conclusions

A better understanding of the U(VI) reduction by the sulfate-reducing bacterium *D. hippei* DSM 8344^T is of high interest not only for the safe disposal of high-level radioactive waste in clay rock, but also for different remediation approaches. In this study, we could verify the reduction of U(VI) by this sulfate-reducing bacterium using different state-of-the-art spectroscopic techniques (TRLFS, UV/Vis, HERFD-XANES and EXAFS). Together with various microscopic techniques, we were able to draw a more profound picture of the ongoing processes. Reduction experiments with different media in combination with luminescence spectroscopic investigations and speciation calculations showed the dependence of

the U(VI) reduction on the initial U(VI) species. The uranyl(VI)-carbonate species could not be reduced by the cells, but in contrast, the uranyl(VI)-lactate complex could be reduced. In latter case, TEM-based analysis of the uranium-incubated cells showed uranium-containing aggregates on the cell surface and indicated the formation of membrane vesicles as a potential defense mechanism against cell encrustation. In connection with an increased amount of U(IV) over time determined by the different spectroscopic methods, a combined association-reduction process can be suggested as a possible interaction mechanism. Moreover, HERFD-XANES measurements verified the presence of U(V) during the experiment, proposing a single-electron transfer as a possible reduction mechanism for this sulfate-reducing genus. To our knowledge, this is the first proof of the occurrence of U(V) during the U(VI) reduction by a sulfate-reducing microorganism. This study shows that the *Desulfosporosinus* species present in clay rock are able to reduce uranium and therefore immobilize it. The significant differences in interaction mechanisms compared to other microorganisms demonstrate the importance of studying the reduction behavior of bacteria of different genera. Furthermore, this study helps to better understand the complexity of redox processes in the environment, assists to close existing gaps in the field of bioremediation and provides new impulses for a comprehensive safeguards concept for a repository for high-level radioactive waste in clay rock.

Acknowledgments

The authors gratefully acknowledge the funding provided by the German Federal Ministry of Education and Research (BMBF) (Grant 02NUK053E) and The Helmholtz Association (Grant SO-093) as well as a partial funding by The Helmholtz-Association, grant PIE-0007 (CROSSING) and the European Union´s Horizon 2020 research and innovation program under the Grant Agreement No. 95237 (SurfBio). We also thank Sindy Kluge for the great support in the laboratory, Sabrina Beutner and Stefanie Bachmann for multiple ICP-MS measurements. Furthermore, we would like to thank Dr. Thomas Kurth and Susanne Kretzschmar from the Center for Regenerative Therapies Dresden (CRTD) for the preparation of the TEM specimens, Falk Lehman from the Helmholtz Institute Freiberg (HIF) for HPLC measurements, and Carola Eckardt and Sylvia Gürtler for ion chromatographic determination of sulfate concentrations. Additionally, the use of the HZDR Ion Beam Cen-

814 ter TEM facilities and the funding of TEM Talos by the German Federal Ministry of Educa-
815 tion and Research (BMBF; grant No. 03SF0451) in the framework of HEMCP are acknowl-
816 edged.

817

References

[1] B. Grambow, *Elements* **2016**, *12*, 239–245.

[2] R. Dohrmann, S. Kaufhold, B. Lundqvist, in *Handb. Clay Sci.* (Eds.: F. Bergaya, G. Lagaly), **2013**, pp. 677–710.

[3] J. Fachinger, M. Den Exter, B. Grambow, S. Holgersson, C. Landesman, M. Titov, T. Podruhzina, *Nucl. Eng. Des.* **2006**, *236*, 543–554.

[4] R. Pusch, *Geological Storage of Highly Radioactive Waste: Current Concepts and Plans for Radioactive Waste Disposal*, Springer Science & Business Media, **2009**.

[5] J. R. Lloyd, L. E. Macaskie, in *Interact. Microorg. with Radionuclides* (Eds.: M.J. Keith-Roach, F.R. Livens), Elsevier, **2002**, pp. 313–381.

[6] S. Selenska-Pobell, M. L. Merroun, in *Prokaryotic Cell Wall Compd. Struct. Biochem.* (Eds.: H. König, H. Claus, A. Varma), Springer-Verlag, Berlin, Heidelberg, **2010**, pp. 483–500.

[7] D. L. Jones, M. B. Andrews, A. N. Swinburne, S. W. Botchway, A. D. Ward, J. R. Lloyd, L. S. Natrajan, *Chem. Sci.* **2015**, *6*, 5133–5138.

[8] A. Bagnoud, K. Chourey, R. L. Hettich, I. De Bruijn, A. F. Andersson, O. X. Leupin, B. Schwyn, R. Bernier-Latmani, *Nat. Commun.* **2016**, *7*, 1–10.

[9] N. Matschiavelli, S. Kluge, C. Podlech, D. Standhaft, G. Grathoff, A. Ikeda-Ohno, L. N. Warr, A. Chukharkina, T. Arnold, A. Cherkouk, *Environ. Sci. Technol.* **2019**, *53*, 10514–10524.

[10] M. Vainshtein, G. Gogotova, H. Hippe, in *Viable Microorg. Permafr.* (Ed.: D. Gilichinsky), Russian Academy Of Science Pushchino Research Center, Pushchino, **1994**, pp. 68–74.

[11] M. Vainshtein, G. Gogotova, H. Hippe, *Microbiology* **1995**, *64*, 436–439.

[12] E. Stackebrandt, C. Sproer, F. A. Rainey, J. Burghardt, O. Päuker, H. Hippe, *Int. J. Syst. Bacteriol.* **1997**, *47*, 1134–1139.

[13] A. Vatsurina, D. Badrutdinova, P. Schumann, S. Spring, M. Vainshtein, *Int. J. Syst. Evol. Microbiol.* **2008**, *58*, 1228–1232.

[14] D. R. Lovley, E. J. P. Phillips, Y. A. Gorby, E. R. Landa, *Nature* **1991**, *350*, 413–416.

[15] B. M. Tebo, A. Y. Obraztsova, *FEMS Microbiol. Lett.* **1998**, *162*, 193–198.

[16] D. R. Lovley, E. J. P. Phillips, *Appl. Environ. Microbiol.* **1992**, *58*, 850–856.

[17] D. R. Lovley, E. E. Roden, E. J. P. Phillips, J. C. Woodward, *Mar. Geol.* **1993**, *113*, 41–53.

[18] K. Pietzsch, B. C. Hard, W. Babel, *J. Basic Microbiol.* **1999**, *39*, 365–372.

[19] R. B. Payne, D. M. Gentry, B. J. Rapp-Giles, L. Casalot, J. D. Wall, *Appl. Environ. Microbiol.* **2002**, *68*, 3129–3132.

[20] P. Junier, E. D. Vecchia, R. Bernier-Latmani, *Geomicrobiol. J.* **2011**, *28*, 483–496.

[21] P. Junier, M. Frutschi, N. S. Wigginton, E. J. Schofield, J. R. Bargar, R. Bernier-Latmani, *Environ. Microbiol.* **2009**, *11*, 3007–3017.

[22] A. Basu, R. A. Sanford, T. M. Johnson, C. C. Lundstrom, F. E. Löffler, *Geochim. Cosmochim. Acta* **2014**, *136*, 100–113.

[23] Y. Suzuki, S. D. Kelly, K. M. Kemner, J. F. Banfield, *Nature* **2002**, *419*, 3849.

[24] Y. Suzuki, S. D. Kelly, K. M. Kemner, J. F. Banfield, *Radiochim. Acta* **2004**, *92*, 11–16.

[25] K. E. Fletcher, M. I. Boyanov, S. H. Thomas, Q. Wu, K. M. Kemner, F. E. Löffler, *Environ. Sci. Technol.* **2010**, *44*, 4705–4709.

[26] R. Bernier-Latmani, H. Veeramani, E. D. Vecchia, P. Junier, J. S. Lezama-Pacheco, E. I. Suvorova, J. O. Sharp, N. S. Wigginton, J. R. Bargar, *Environ. Sci. Technol.* **2010**, *44*, 9456–9462.

[27] J. R. Postgate, *The Sulphate-Reducing Bacteria*, Cambridge University Press, Cambridge, **1984**.

[28] D. R. Lovley, P. K. Widman, J. C. Woodward, E. J. P. Phillips, *Appl. Environ. Microbiol.* **1993**, *59*, 3572–3576.

[29] P. Wersin, O. X. Leupin, S. Mettler, E. C. Gaucher, U. Mäder, P. De Cannière, A. Vinsot, H. E. Gäbler, T. Kunimaro, K. Kiho, et al., *Appl. Geochemistry* **2011**, *26*, 931–953.

873 [30] K. U. Ulrich, A. Singh, E. J. Schofield, J. R. Bargar, H. Veeramani, J. O. Sharp, R.
874 Bernier-Latmani, D. E. Giammar, *Environ. Sci. Technol.* **2008**, *42*, 5600–5606.

875 [31] E. J. Schofield, H. Veeramani, J. O. Sharp, E. Suvorova, R. Bernier-Latmani, A. Mehta,
876 J. Stahlman, S. M. Webb, D. L. Clark, S. D. Conradson, et al., *Environ. Sci. Technol.*
877 **2008**, *42*, 7898–7904.

878 [32] J. O. Sharp, E. J. Schofield, H. Veeramani, E. I. Suvorova, D. W. Kennedy, M. J.
879 Marshall, A. Mehta, J. R. Bargar, R. Bernier-Latmani, *Environ. Sci. Technol.* **2009**, *43*,
880 8295–8301.

881 [33] G. F. Vettese, K. Morris, L. S. Natrajan, S. Shaw, T. Vitova, J. Galanzew, D. L. Jones, J.
882 R. Lloyd, *Environ. Sci. Technol.* **2020**, *54*, 2268–2276.

883 [34] J. C. Renshaw, L. J. C. Butchins, F. R. Livens, I. May, J. M. Charnock, J. R. Lloyd,
884 *Environ. Sci. Technol.* **2005**, *39*, 5657–5660.

885 [35] G. R. Choppin, P. J. Wong, *Aquat. Geochemistry* **1998**, *4*, 77–101.

886 [36] W. Runde, *Geochemistry Soil Radionuclides* **2015**, *103*, 21–44.

887 [37] P. L. Arnold, J. B. Love, D. Patel, *Coord. Chem. Rev.* **2009**, *253*, 1973–1978.

888 [38] G. Nocton, P. Horeglad, V. Vetere, J. Pécaut, L. Dubois, P. Maldivi, N. M. Edelstein, M.
889 Mazzanti, *J. Am. Chem. Soc.* **2010**, *132*, 495–508.

890 [39] M. F. Schettini, G. Wu, T. W. Hayton, *Inorg. Chem.* **2009**, *48*, 11799–11808.

891 [40] T. I. Docrat, J. F. W. Mosselmans, J. M. Charnock, M. W. Whiteley, D. Collison, F. R.
892 Livens, C. Jones, M. J. Edmiston, *Inorg. Chem.* **1999**, *38*, 1879–1882.

893 [41] A. Ikeda, C. Hennig, S. Tsushima, K. Takao, Y. Ikeda, A. C. Scheinost, G. Bernhard,
894 *Inorg. Chem.* **2007**, *46*, 4212–4219.

895 [42] K. Mizuoka, I. Grenthe, Y. Ikeda, *Inorg. Chem.* **2005**, *44*, 4472–4474.

896 [43] R. Faizova, R. Scopelliti, A. S. Chauvin, M. Mazzanti, *J. Am. Chem. Soc.* **2018**, *140*,
897 13554–13557.

898 [44] H. E. Roberts, K. Morris, G. T. W. Law, J. F. W. Mosselmans, P. Bots, K. Kvashnina, S.
899 Shaw, *Environ. Sci. Technol. Lett.* **2017**, *4*, 421–426.

900 [45] S. Tsarev, R. N. Collins, A. Fahy, T. D. Waite, *Environ. Sci. Technol.* **2016**, *50*, 2595–

2601.

[46] S. Tsarev, R. N. Collins, E. S. Ilton, A. Fahy, T. D. Waite, *Environ. Sci. Nano* **2017**, *4*, 1304–1313.

[47] I. Pidchenko, K. O. Kvashnina, T. Yokosawa, N. Finck, S. Bahl, D. Schild, R. Polly, E. Bohnert, A. Rossberg, J. Göttlicher, et al., *Environ. Sci. Technol.* **2017**, *51*, 2217–2225.

[48] E. S. Ilton, P. S. Bagus, *Surf. Interface Anal.* **2011**, *43*, 1549–1560.

[49] T. A. Marshall, K. Morris, G. T. W. Law, J. F. W. Mosselmans, P. Bots, H. Roberts, S. Shaw, *Mineral. Mag.* **2015**, *79*, 1265–1274.

[50] K. O. Kvashnina, S. M. Butorin, P. Martin, P. Glatzel, *Phys. Rev. Lett.* **2013**, *111*, 253002.

[51] K. O. Kvashnina, S. M. Butorin, *Chem. Commun.* **2022**, *58*, 327–342.

[52] K. P. Nevin, K. T. Finneran, D. R. Lovley, *Appl. Environ. Microbiol.* **2003**, *69*, 3672–3675.

[53] Y. Suzuki, S. D. Kelly, K. M. Kemner, J. F. Banfield, *Appl. Environ. Microbiol.* **2003**, *69*, 1337–1346.

[54] E. Cardenas, W. M. Wu, M. B. Leigh, J. Carley, S. Carroll, T. Gentry, J. Luo, D. Watson, B. Gu, M. Ginder-Vogel, et al., *Appl. Environ. Microbiol.* **2008**, *74*, 3718–3729.

[55] J. M. Senko, G. Zhang, J. T. McDonough, M. A. Bruns, W. D. Burgos, *Geomicrobiol. J.* **2009**, *26*, 71–82.

[56] S. Ramamoorthy, H. Sass, H. Langner, P. Schumann, R. M. Kroppenstedt, S. Spring, J. Overmann, R. F. Rosenzweig, *Int. J. Syst. Evol. Microbiol.* **2006**, *56*, 2729–2736.

[57] A. Courdouan, I. Christl, S. Meylan, P. Wersin, R. Kretzschmar, *Appl. Geochemistry* **2007**, *22*, 2926–2939.

[58] S. Hilpmann, M. Bader, R. Steudtner, K. Müller, T. Stumpf, A. Cherkouk, *PLoS One* **2022**, *17*, e0262275.

[59] J. Jessat, H. Moll, W. A. John, M. L. Bilke, R. Hübner, J. Kretzschmar, R. Steudtner, B. Drobot, T. Stumpf, S. Sachs, *J. Hazard. Mater.* **2022**, *439*, DOI

10.1016/j.jhazmat.2022.129520.

[60] M. Bader, A. Rossberg, R. Steudtner, B. Drobot, K. Großmann, M. Schmidt, N. Musat, T. Stumpf, A. Ikeda-Ohno, A. Cherkouk, *Environ. Sci. Technol.* **2018**, *52*, 12895–12904.

[61] R. Steudtner, S. Sachs, K. Schmeide, V. Brendler, G. Bernhard, *Radiochim. Acta* **2011**, *99*, 687–692.

[62] M. Völkner, T. Kurth, M. O. Karl, *Methods Mol. Biol.* **2019**, *1834*, 119–141.

[63] M. Völkner, T. Kurth, J. Schor, L. J. A. Ebner, L. Bardtke, C. Kavak, J. Hackermüller, M. O. Karl, *Front. Cell Dev. Biol.* **2021**, *9*, 645704.

[64] K. O. Kvashnina, Y. O. Kvashnin, S. M. Butorin, *J. Electron Spectros. Relat. Phenomena* **2014**, *194*, 27–36.

[65] P. A. Lee, P. H. Citrin, P. Eisenberger, B. M. Kincaid, *Rev. Mod. Phys.* **1981**, *53*, 769–806.

[66] A. C. Scheinost, J. Claussner, J. Exner, M. Feig, S. Findeisen, C. Hennig, K. O. Kvashnina, D. Naudet, D. Prieur, A. Rossberg, et al., *J. Synchrotron Radiat.* **2021**, *28*, 333–349.

[67] K. O. Kvashnina, A. C. Scheinost, *J. Synchrotron Radiat.* **2016**, *23*, 836–841.

[68] G. N. George, I. J. Pickering, **1995**.

[69] A. Ankudinov, B. Ravel, *Phys. Rev. B - Condens. Matter Mater. Phys.* **1998**, *58*, 7565–7576.

[70] Y. Dusausoy, N. E. Ghermani, R. Podor, M. Cuney, *Eur. J. Mineral.* **1996**, *8*, 667–673.

[71] A. Rossberg, T. Reich, G. Bernhard, *Anal. Bioanal. Chem.* **2003**, *376*, 631–638.

[72] E. R. Malinowski, *Factor Analysis in Chemistry*, John Wiley & Sons, New York, **1991**.

[73] N. Mayodormo, D. M. Rodriguez, A. Rossberg, H. Foerstendorf, K. Heim, V. Brendler, K. Müller, *Chem. Eng. J.* **2021**, *408*, 127265.

[74] B. H. Jeon, S. D. Kelly, K. M. Kemner, M. O. Barnett, W. D. Burgos, B. A. Dempsey, E. E. Roden, *Environ. Sci. Technol.* **2004**, *38*, 5649–5655.

[75] D. Brady, A. Stoll, J. R. Duncan, *Environ. Technol.* **1994**, *15*, 429–438.

[76] B. Volesky, H. A. May-Phillips, *Appl. Microbiol. Biotechnol.* **1995**, *42*, 797–806.

[77] R. J. Silva, H. Nitsche, *Ract* **1995**, *70–71*, 377–396.

[78] J. E. Banaszak, B. E. Rittmann, D. T. Reed, *J. Radioanal. Nucl. Chem.* **1999**, *241*, 385–435.

[79] R. Klemps, H. Cypionka, F. Widdel, N. Pfennig, *Arch. Microbiol.* **1985**, *143*, 203–208.

[80] B. Drobot, R. Steudtner, J. Raff, G. Geipel, V. Brendler, S. Tsushima, *Chem. Sci.* **2015**, *6*, 964–972.

[81] P. P. Shao, L. R. Comolli, R. Bernier-Latmani, *Minerals* **2014**, *4*, 74–88.

[82] M. M. Clark, M. D. Paxhia, J. M. Young, M. P. Manzella, G. Reguera, *Appl. Environ. Microbiol.* **2021**, *87*, 1–17.

[83] T. Nagai, T. Fujii, O. Shirai, H. Yamana, *J. Nucl. Sci. Technol.* **2004**, *41*, 690–695.

[84] P. Wang, F. Dong, D. He, S. Liu, N. Chen, T. Huo, *RSC Adv.* **2021**, *11*, 23241–23248.

[85] B. E. Cowie, J. M. Purkis, J. Austin, J. B. Love, P. L. Arnold, *Chem. Rev.* **2019**, *119*, 10595–10637.

[86] Z. Pan, B. Bártová, T. LaGrange, S. M. Butorin, N. C. Hyatt, M. C. Stennett, K. O. Kvashnina, R. Bernier-Latmani, *Nat. Commun.* **2020**, *11*, 1–12.

[87] E. R. Malinowski, *Anal. Chim. Acta* **1978**, *103*, 339–354.

[88] I. Feldmann, C. A. North, H. B. Hunter, *J. Phys. Chem.* **1960**, *64*, 1224–1230.

[89] I. Feldmann, J. R. Havill, W. F. Neuman, *J. Am. Chem. Soc.* **1954**, *76*, 4726–4732.

[90] K. S. Rajan, A. E. Martell, *J. Inorg. Nucl. Chem.* **1964**, *26*, 1927–1944.

[91] P. G. Allen, D. K. Shuh, J. J. Bucher, N. M. Edelstein, T. Reich, M. A. Denecke, H. Nitsche, *Inorg. Chem.* **1996**, *35*, 784–787.

[92] C. Lucks, Untersuchungen Zur Struktur von Wassergelösten Und an Hämatit Sorbierten Uran(VI)-Komplexen Mit Aliphatischen (Hydroxy-) Carbonsäuren: Kombination Verschiedener Spektroskopischer Methoden Mit Faktoranalyse Und Quantenchemischen Berechnungen, Technische Universität Dresden, **2012**.

[93] G. G. Li, F. Bridges, C. H. Booth, *Phys. Rev. B* **1995**, *52*, 6332–6348.

[94] P. Fornasini, R. Grisenti, *J. Synchrotron Radiat.* **2015**, *22*, 1242–1257.

[95] J. Kretzschmar, S. Tsushima, C. Lucks, E. Jäckel, R. Meyer, R. Steudtner, K. Müller, A. Rossberg, K. Schmeide, V. Brendler, *Inorg. Chem.* **2021**, *60*, 7998–8010.

[96] J. Kretzschmar, S. Tsushima, B. Drobot, R. Steudtner, K. Schmeide, T. Stumpf, *Chem. Commun.* **2020**, *56*, 13133–13136.

[97] E. Grabias, M. Majdan, *J. Radioanal. Nucl. Chem.* **2017**, *313*, 455–465.

[98] S. Tsushima, A. Rossberg, A. Ikeda, K. Müller, A. C. Scheinost, *Inorg. Chem.* **2007**, *46*, 10819–10826.

[99] L. Newsome, K. Morris, S. Shaw, D. Trivedi, J. R. Lloyd, *Chem. Geol.* **2015**, *409*, 125–135.

[100] L. Newsome, K. Morris, D. Trivedi, A. Bewsher, J. R. Lloyd, *Environ. Sci. Technol.* **2015**, *49*, 11070–11078.

[101] L. Downward, C. H. Booth, W. W. Lukens, F. Bridges, *AIP Conf. Proc.* **2007**, *882*, 129–131.